HEDL-SA-2158

MASTER

CONF-801072--5

RADIATION-INDUCED EVOLUTION OF AUSTENITE MATRIX IN SILICON-MODIFIED AISI 316 ALLOYS

FA Garner
HR Brager

IRRADIATION PHASE STABILITY SYMPOSIUM

October 5-9, 1980 Pittsburgh, PA

HANFORD ENGINEERING DEVELOPMENT LABORATORY
Operated by Westinghouse Hanford Company, a subsidiary of Westinghouse Electric Corporation, under the Department of Energy Contract No. DE-AC14-76FF02170
P.O. Box 1970, Richland, Washington 99352

DISCLAIMER

RADIATION-INDUCED EVOLUTION OF THE AUSTENITE MATRIX IN SILICON-MODIFIED AISI 316 ALLOYS*

H. R. Brager and F. A. Garner

Hanford Engineering Development Laboratory
Richland, Washington

The microstructures of a series of silicon-modified AISI 316 alloys irradiated to fast neutron fluences of about 2-3 and 10 x 10^{22} n/cm^2 (E > 0.1 MeV) at temperatures ranging from 400°C to 600°C have been examined. The irradiation of AISI 316 leads to an extensive repartition of several elements, particularly nickel and silicon, between the matrix and various precipitate phases. The segregation of nickel at void and grain boundary surfaces at the expense of other faster-diffusing elements is a clear indication that one of the mechanisms driving the microchemical evolution is the Inverse Kirkendall effect. There is evidence that at any one sink this mechanism is in competition with the solute drag process associated with interstitial gradients.

At low silicon levels, increasing the silicon content depresses void nucleation and is manifest as an increased incubation fluence. Increases in the silicon content above 0.5% reduce the matrix nickel content by increases in the amount of nickel- and silicon-rich phases, resulting in higher swelling rates. Large additions of silicon cause progressively larger fractions of the austenite matrix to transform to ferrite as the matrix nickel level decreases. The austenite to ferrite transformation is resisted near nickel-rich void surfaces.

* This work was supported by the Department of Energy under Contract No. DE-AC14-76FF02170.

Introduction

The irradiation-induced phase development that occurs in AISI 316 leads to extensive changes in the composition of the austenite matrix (1-11). These changes have been shown to account for much of the observed behavior of this steel in response to variations in composition, preirradiation thermal-mechanical treatment and environmental variables such as displacement rate, temperature and stress (12-15). One of the three major participants of this evolution has been shown to be the element silicon (5,12), which appears both to suppress void nucleation while in solution (16) and to provide a chemical reservoir for coprecipitation with the element nickel from the austenite matrix. Nickel has also been identified as the second of three major participants in the microchemical evolution of this steel; carbon is the third.

In this paper, the response of the microchemical evolution of AISI 316 to variations in silicon content will be examined in two separate irradiation experiments involving the same alloys. The details of the first experiment, designated MV-I, have been described previously in a paper focusing primarily on the dependence of radiation-induced density changes of AISI 316 on the level of silicon and other elements (17). The microstructures of some of these specimens was examined in 1974 but have not been previously reported in the open literature. Many of the specimens irradiated in the first experiment were then reirradiated to higher fluence in a second experiment designated MV-II (18). In the period between the two experiments a new analytical tool has come into prominence, namely scanning transmission electron microscopy in conjunction with energy dispersive X-ray (EDX) microanalysis techniques. Selected specimens from the MV-II experiment have been examined to provide a fuller insight on the microchemical evolution than was possible with the MV-I experiment.

Experimental Details

Unstressed specimens of the MV-I experiment were contained in sodium-filled capsules and irradiated in the EBR-II fast reactor. The elemental compositions of each of the five silicon-series alloys examined and discussed in this report, shown in Table 1, are for alloys in the solution annealed (1925°F/water quenched) condition. The four irradiation temperatures ranged from ∿400 to ∿800°C with fluences varying from 2 to 4 x 10^{22} n/cm^2 (E >0.1 MeV). Conventional electron microscopy and specimen thinning techniques were employed in this first study. Specimens at ∿800°C exhibited no swelling.

Three irradiation temperatures were represented in the MV-II experiment: 400, 510 and 620°C. The specimens examined and reported in this second study were the same five silicon series alloys examined in MV-I, but were exposed to an additional increment of neutron fluence of between 7 to 8 x 10^{22} n/cm^2 (E >0.1 MeV). Specimens of both the solution annealed and 20% cold worked conditions were examined and the microanalysis of local elemental composition was performed using techniques and equipment described elsewhere (4).

Results of MV-I Experiment

Figures 1(a) and 2 show that voids were observed in all five alloys at 405°C and a fluence of 1.8 x 10^{22} n/cm^2, that the void number density diminished with increasing silicon, and that swelling declined linearly with silicon content. The mean void sizes were essentially equal in all five alloys. Typical microstructures are shown in Figure 2, which shows that small precipitates also form and that their density and mean size increase with silicon content. These precipitates were small cubes with sides parallel to <100> directions in the matrix. Voids appear to be attached to the precipitates only at the higher silicon levels.

Alloy	Density, g/cm^3	Element, Weight %					
		C	Mn	Si	P	S	Cr
25	7.99698	0.046	0.95	0.01	0.010	0.008	16.88
26	7.96249	0.045	0.94	0.48	0.009	0.008	17.00
27	7.92499	0.045	0.94	0.95	0.011	0.007	17.06
28	7.88573	0.044	0.93	1.47	0.010	0.008	17.07
29	7.85047	0.045	0.94	1.96	0.010	0.007	17.13

Alloy	Density, g/cm^3	Element, Weight %					
		Ni	Mo	Cu	Co	B	N
25	7.99698	11.98	2.31	0.10	0.11	0.0011	0.052
26	7.96249	12.12	2.34	0.11	0.11	0.0010	0.054
27	7.92499	12.19	2.35	0.10	0.11	0.0007	0.049
28	7.88573	12.30	2.38	0.10	0.11	0.0007	0.054
29	7.85047	12.39	2.41	0.11	0.11	0.0010	0.050

Table 1. Alloy Compositions: Silicon Variations

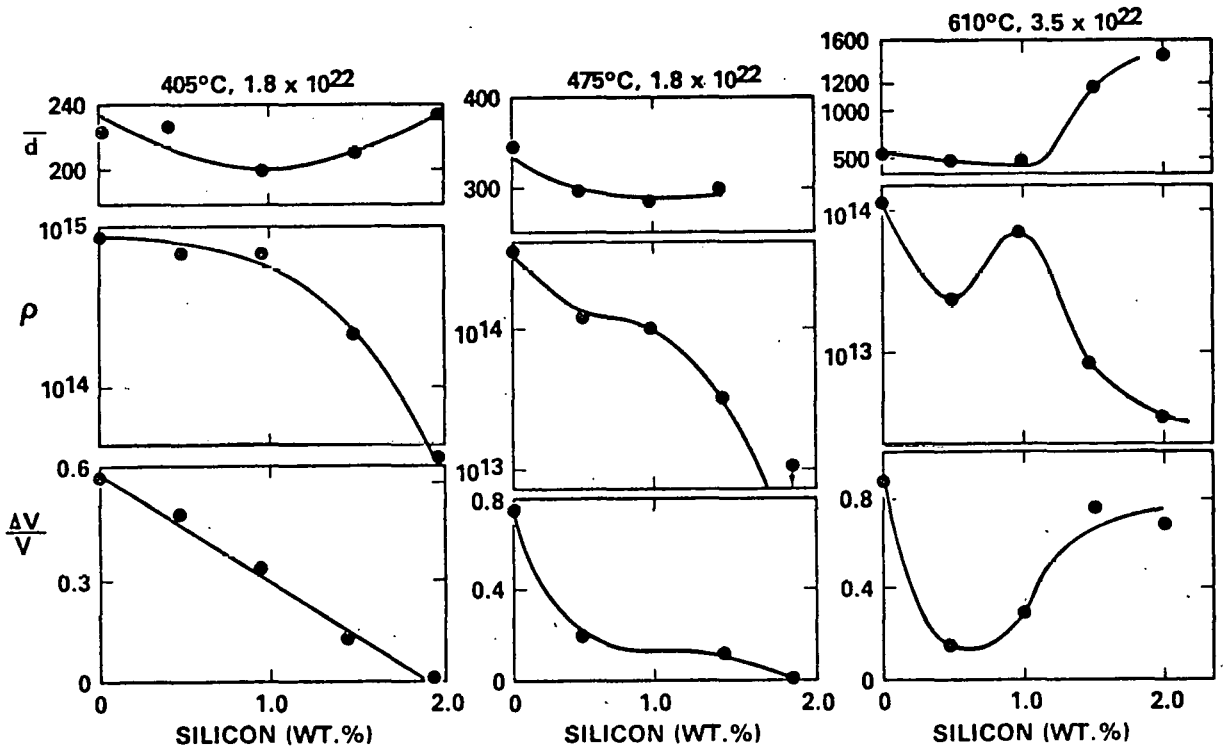

Fig. 1 - Void characteristics observed in the MV-I silicon series experiment.

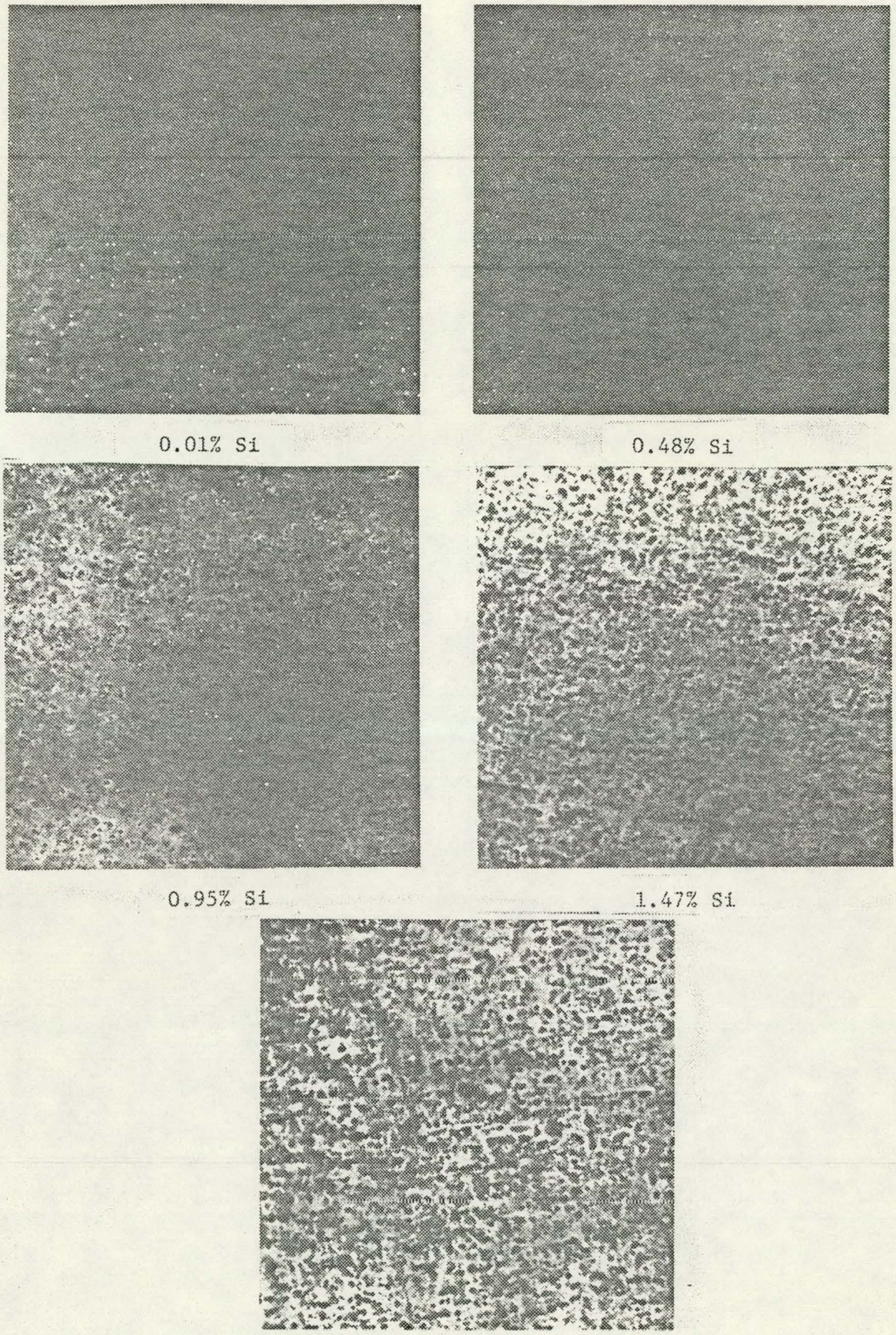

Fig. 2 - Typical bright field micrographs showing void and precipitate microstructures for specimens irradiated at 405°C to a fluence of 1.8 x 10^{22} n/cm^2.

At 475°C a similar trend was observed, as shown in Figures 1(b) and 3. Once again, the void sizes are essentially independent of silicon level, and the void number density declines even more steeply with additional silicon than was observed at 405°C. As shown in Figure 3, the precipitates are now much larger than those observed at 405°C. The void nucleation seems to occur heterogeneously at the lowest silicon concentration, and varying degrees of inhomogeneity are observed in different areas of the specimen. At low silicon levels, the voids appear to have nucleated on dislocations that existed prior to irradiation.

At 610°C the tendency toward heterogeneous void nucleation becomes very pronounced, as shown in Figure 4. At low silicon levels voids again appear to nucleate on pre-existing dislocations, and at higher silicon concentrations voids have nucleated almost exclusively on precipitates. There appears to be two types of precipitate-assisted void nucleation events, however. Small voids are in general associated with small rod-shaped precipitates and large voids are found on the large blocky precipitates, as shown in Figure 5.

The void number density and total swelling at 610°C are not monotonically decreasing functions of silicon concentration, in contrast to the behavior observed at 405 and 475°C. As shown in Figure 1(c), these parameters exhibit an increase between 0.5 and 1.0% silicon. This change in behavior is coincident with the onset of large blocky precipitate formation. As illustrated in the last micrograph in Figure 4, these precipitates dominate the contrast when imaged at 100 keV. The micrograph in Figure 6 demonstrates the greater penetration available on a 1.0 MeV microscope and better illustrates the nature of the high density of precipitates that form under these conditions. The lattice parameter of these fcc precipitates was found to be 1.058 ±0.02 nm. They were assumed at that time to be complex carbosilicides of unspecified identity.

Results of MV-II Silicon Series Experiment

The swelling levels (determined by immersion density measurements) of these specimens are shown in Figure 7. Note that for irradiation above 500°C, the swelling at these higher fluences is no longer monotonically decreasing with silicon content, but exhibits two reversals in behavior.(3,18)

At 620°C and 1.2 x 10^{23} n/cm^2 (E >0.1 MeV) the annealed specimen with 0.01% silicon contained a single-peaked distribution of very large voids (∿100 nm diameter) but no extensive precipitation. At this large swelling level (14%), the nickel segregates to the void surfaces. This segregation performs the nickel removal function normally accomplished by precipitates at higher silicon levels. Line-of-sight EDX measurements at voids indicated nickel concentrations as large as 19% but the actual nickel level at the void surface is much larger than 19% (4). There was no consistent enrichment or depletion of silicon or molybdenum at the void surface. A depletion of chromium and iron at the surface was observed.

In the annealed specimen alloyed with 0.5% silicon irradiated at 620°C and 1.2 x 10^{23} n/cm^2, the swelling was much lower (∿1%) and there were the large carbosilicides and Laves precipitates typically observed in this alloy. During irradiation these precipitates were enriched in nickel and silicon as observed in earlier studies.(1-6) Laves is not rich in these elements in thermally aged specimens. The voids showed enriched nickel concentrations at their surfaces and the matrix nickel content was on the order of 11 to 12%.

The annealed specimen was 0.95% silicon at 620°C was not examined but the 1.47 and 1.96% silicon specimens were examined. Tilting of these specimens in the microscope induced substantial perturbations in the electron beam and indicated that the specimens had developed ferromagnetic phases. In the 1.47%

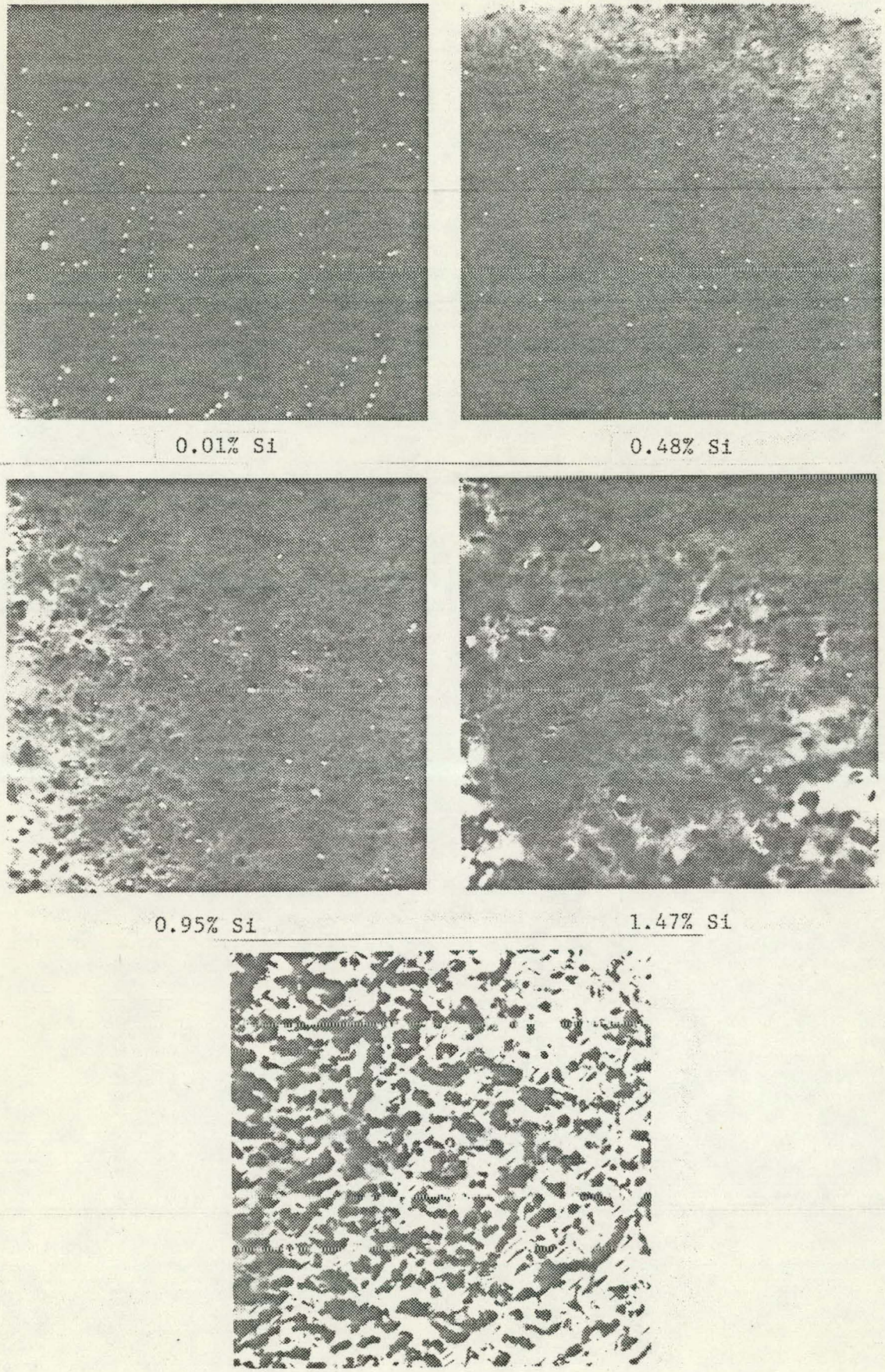

Fig. 3 - Typical bright field micrographs showing void and precipitate microstructures for specimens irradiated at 475°C to a fluence of 1.8 x 10^{22} n/cm^2.

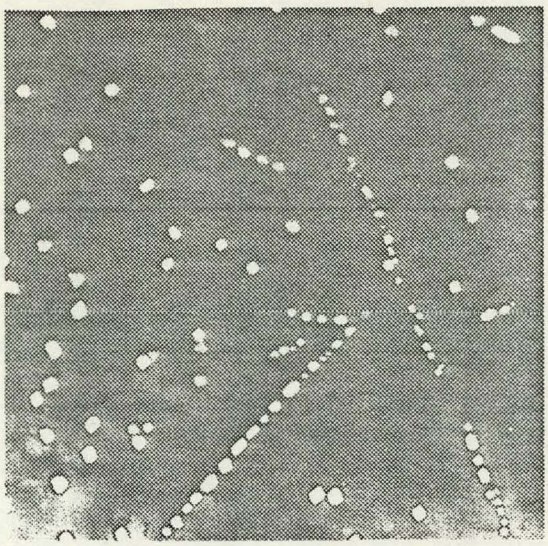

0.01% Si

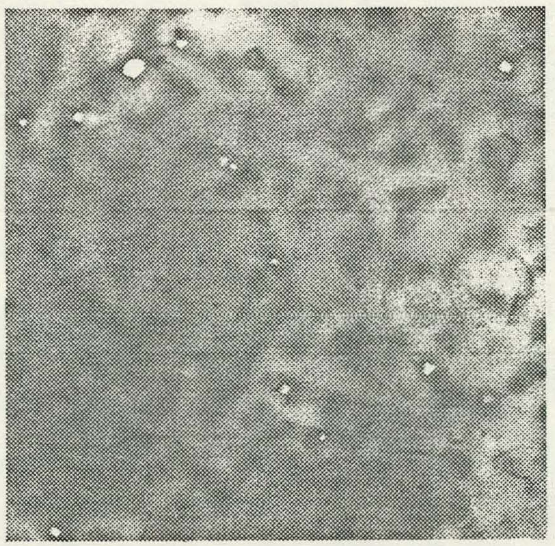

0.48% Si

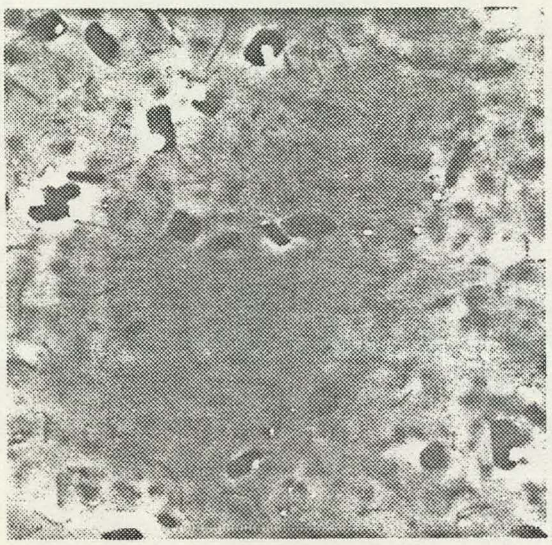

0.95% Si

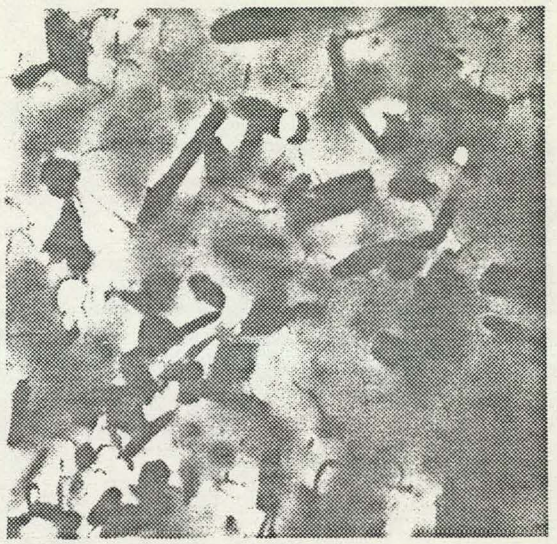

1.47% Si

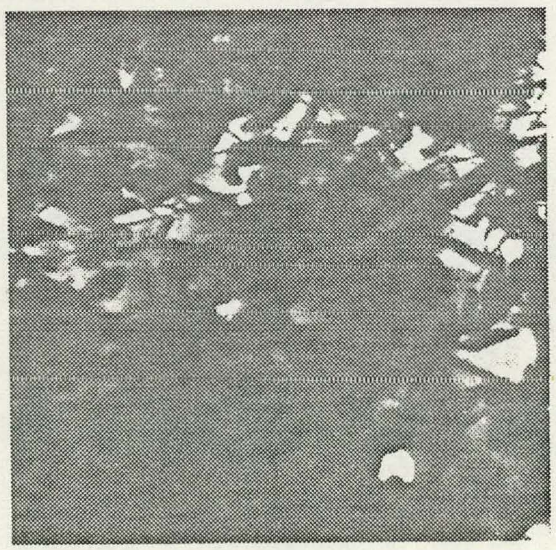

1.96% Si

Fig. 4 - Typical bright field micrographs showing void and precipitate microstructures for specimens irradiated at 610°C to a fluence of 3.5 x 10^{22} n/cm^2.

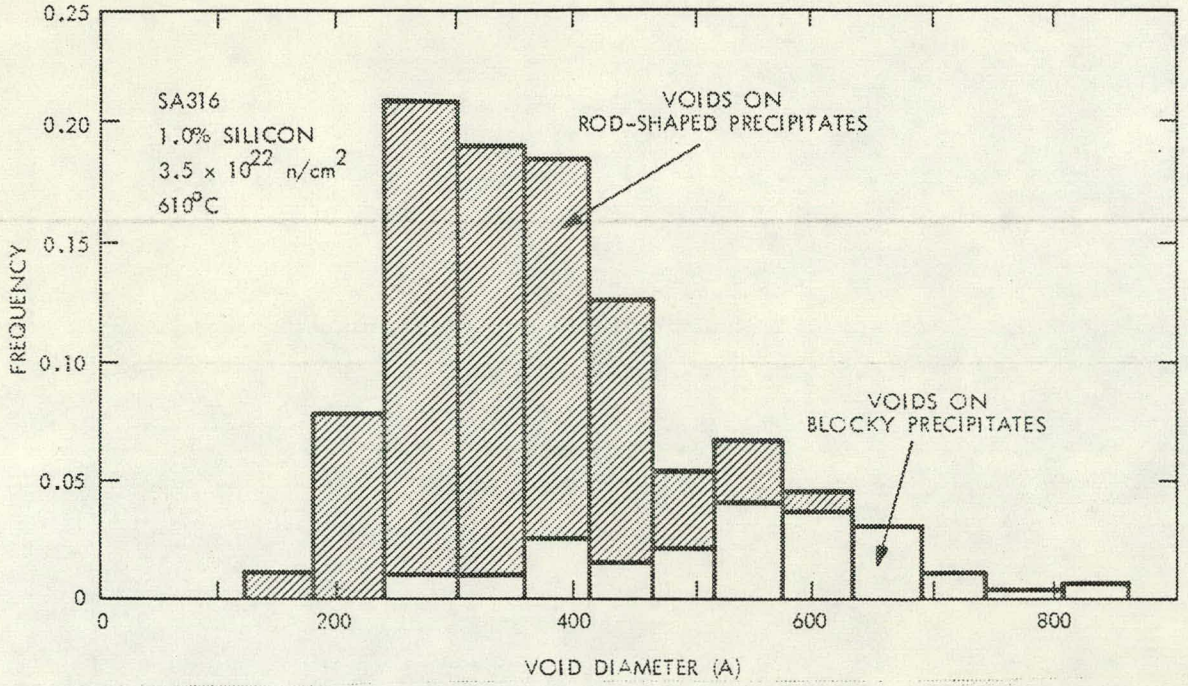

Fig. 5 - The relationship of void size distribution and type of precipitate with which voids are associated.

Fig. 6 - Precipitate microstructure in the 2% silicon alloy after irradiation at 610°C to a fluence of 3.5 x 10^{22} n/cm^2 (imaged with 1.0 MeV electrons).

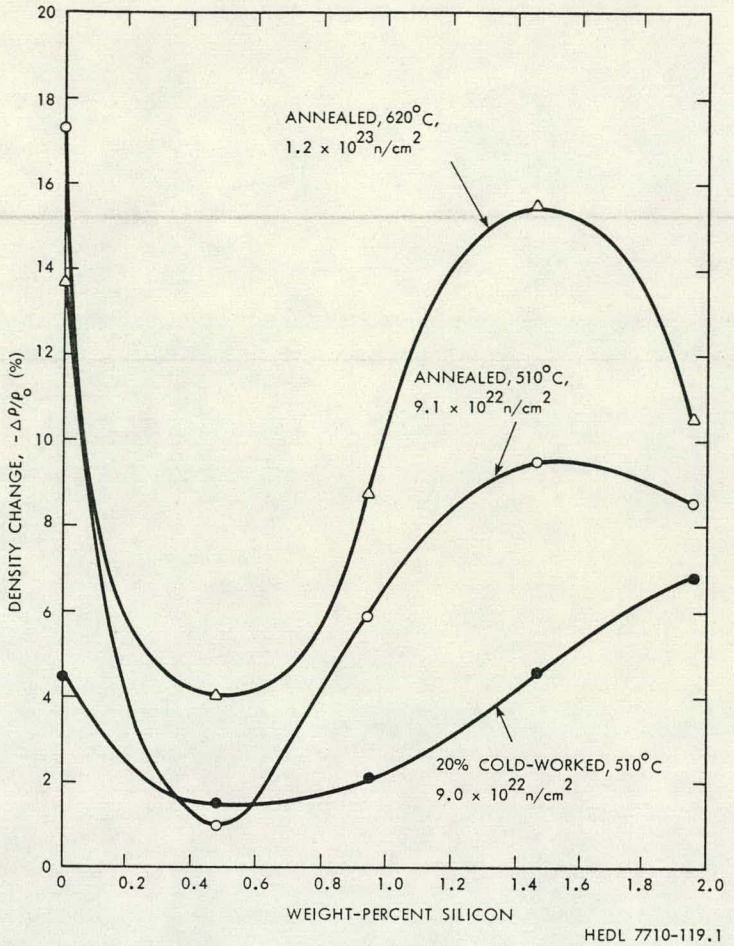

Fig. 7 - Density changes observed in the silicon series alloys irradiated in the MV-II experiment (3,18). See reference 18 for data at 400°C.

silicon specimen, 25 to 50% of the specimen had transformed to ferrite. The remaining austenite contained a high density of a variety of phases, all silicon-rich including surprisingly γ' (50 nm, 10^{15} cm^{-3}), as shown in Figure 8. These phases comprised 20 to 25% of the alloy volume. The ferrite tended to form in regions which did not contain voids. In some areas where extensive ferrite formation had occurred, the voids remained encased in austenite shells, totally surrounded by ferrite. In regions where voids comprised a substantial fraction of the volume, austenite regions of complex shapes related to the void distribution tended to persist against the austenite → ferrite transformation. Examples of both the austenite shells around single voids and the envelopes around void complexes are shown in Figure 9.

In the 1.96% silicon specimen irradiated at 620°C to 1.2 x 10^{23} n/cm^2, the fraction of austenite transformed to ferrite was larger than 50% and the level of precipitation had again increased. The γ' phase was again (unexpectedly at this temperature) observed in the austenite phase. Analysis of the silicon-rich precipitates that were not γ' was attempted *in situ* and gave average compositions (wt. %) of 35% Ni, 10% Mo, 20% Si, 20% Fe, and 10% Cr. The crystal structure of most of the precipitates analyzed was that of Laves. The nickel concentration in the matrix was measured to be as low as 6% in both austenite and ferrite phases. Due to the complexity of the microstructure, the *in situ* determination of elemental compositions was deemed to be somewhat suspect. Therefore, an extraction replication was performed. Analysis of eight separate precipitates showed them to be essentially identical at 45% Ni, 15% Mo, 10% Si, 20% Fe, and 10% Cr. These precipitates also

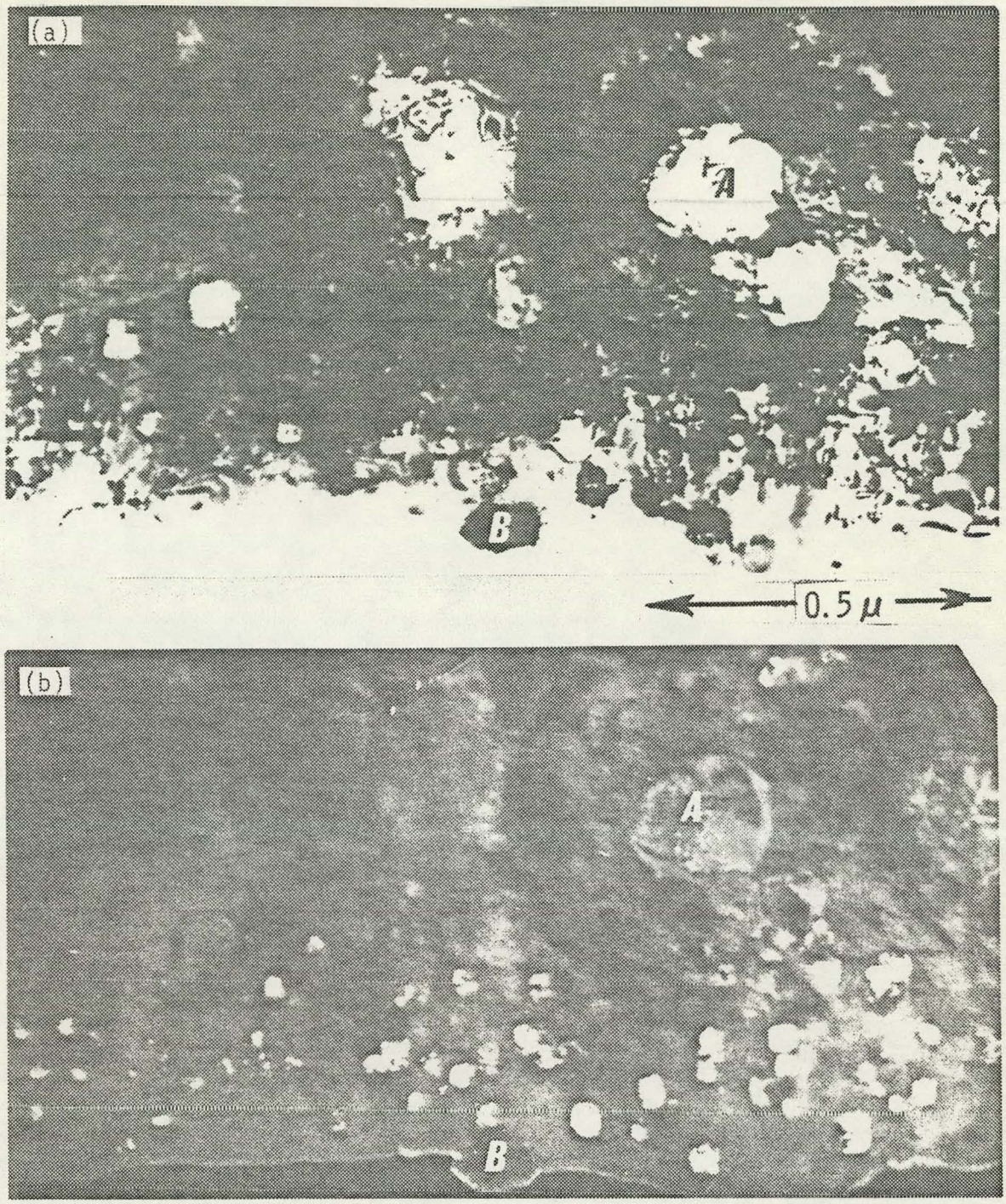

Fig. 8 - Micrographs showing complex microstructure developed in the 1.47% silicon alloy after irradiation at 620°C to 12.0 x 10^{22} n/cm^2 (E >0.1 MeV). (a) Bright field, (b) dark field showing presence of γ' precipitates in austenite regions along foil edge, and (c) dark field showing ferrite regions surrounding austenite-coated voids (next page).

had uniform concentrations throughout their volume, with no near-surface concentration gradients.

Two specimens irradiated at 510°C were also examined. The first was the 0.48% silicon alloy in the 20% cold worked condition which had been irradiated to 9.0 x 10^{22} n/cm^2. It contained both the γ' and "carbosilicide" phase normally observed at this temperature and fluence. An annealed specimen of this alloy had been irradiated to a slightly higher fluence (9.1 x 10^{22} n/cm^2) at

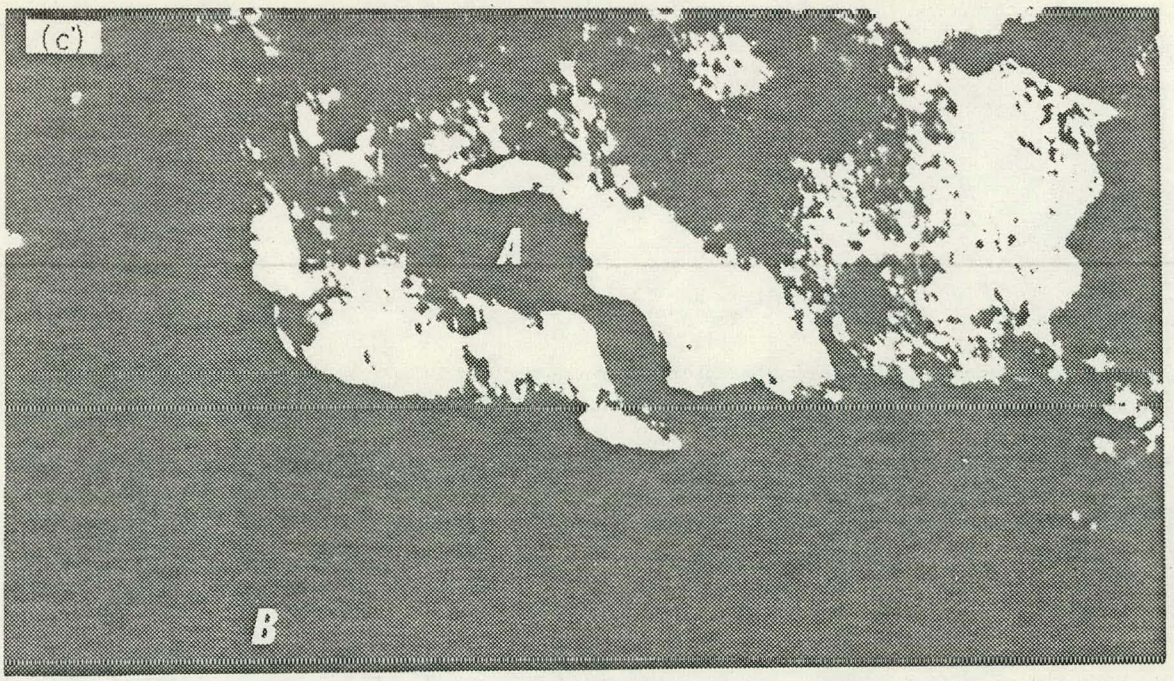

Fig. 8(c) - Dark field showing ferrite regions surrounding coated voids.

the same temperature. Comparable amounts of γ' and "carbosilicides" had developed in both specimens, an observation which is consistent with their nominally identical swelling levels. The "carbosilicides" did not have enrichment of nickel and silicon levels with respect to the overall matrix composition, however. There was substantial enrichment of chromium and molybdenum in these precipitates.

The γ' precipitates in specimens irradiated at 510°C are somewhat smaller than the width of the electron beam in size and exist at high densities. Thus it is not possible to determine the matrix nickel content directly. When concentration levels are measured across a grain boundary, however, several interesting features of the matrix composition can be observed. As shown in Figure 10, the apparent nickel concentration decreases in the vicinity of the grain boundary with a small secondary increase at the boundary itself. This profile is somewhat misleading in that the apparent decrease in nickel is due to the presence of a zone denuded of the nickel-rich γ' phase near the boundary. This denuded zone was observed to be about 100 nm on each side of the boundary. The actual matrix composition is thus in the 9 to 10% range expected for this alloy. Note that there is a small enrichment of nickel at the boundary similar to that observed at void surfaces. There is also an unexpected enrichment in the molybdenum concentration. The chromium profile exhibits a depletion near the boundary while iron exhibits a concentration increase. These trends were confirmed at other grain boundary positions.

Discussion

The MV-I data show that at low fluence, silicon appears to inhibit void nucleation in neutron irradiations at all temperatures studied. With the exception of high (≥1 wt.%) silicon levels at 610°C, this suppression of nucleation leads to a decrease in swelling. Increasing the concentration of silicon also leads to extensive precipitation of various phases, all rich in silicon and nickel. The tendency toward heterogeneous nucleation at high temperatures and high silicon levels is another indication of the difficulty of nucleating voids under these conditions. There is no information in the MV-I data to indicate whether the suppression of nucleation by silicon is a temporary (low fluence) or permanent phenomenon, however.

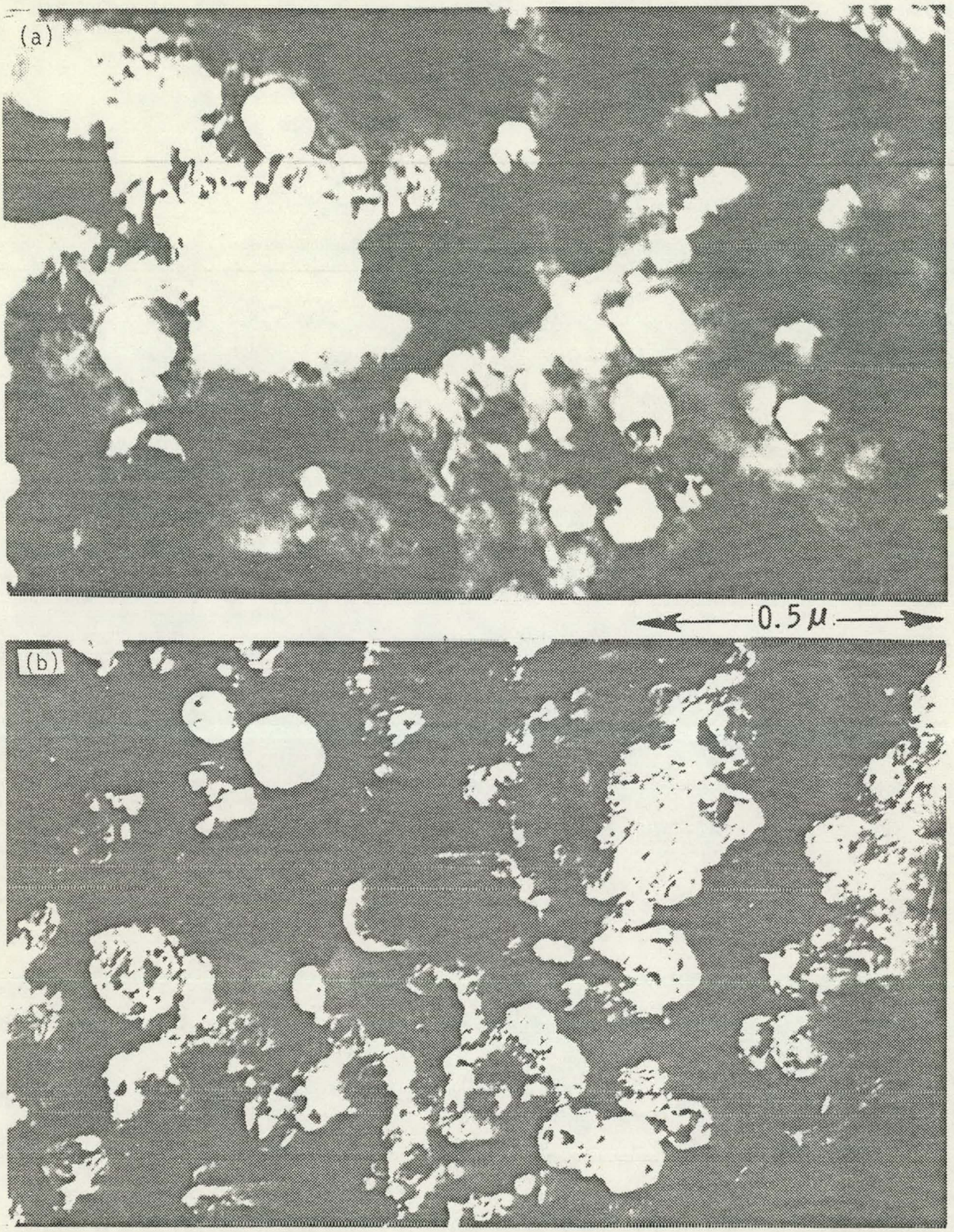

Fig. 9 - Bright field and dark field micrographs showing complex phase development in 1.47% silicon alloy at 620°C. Note the austenite shells, Figure b, around some isolated voids and also connecting voided regions.

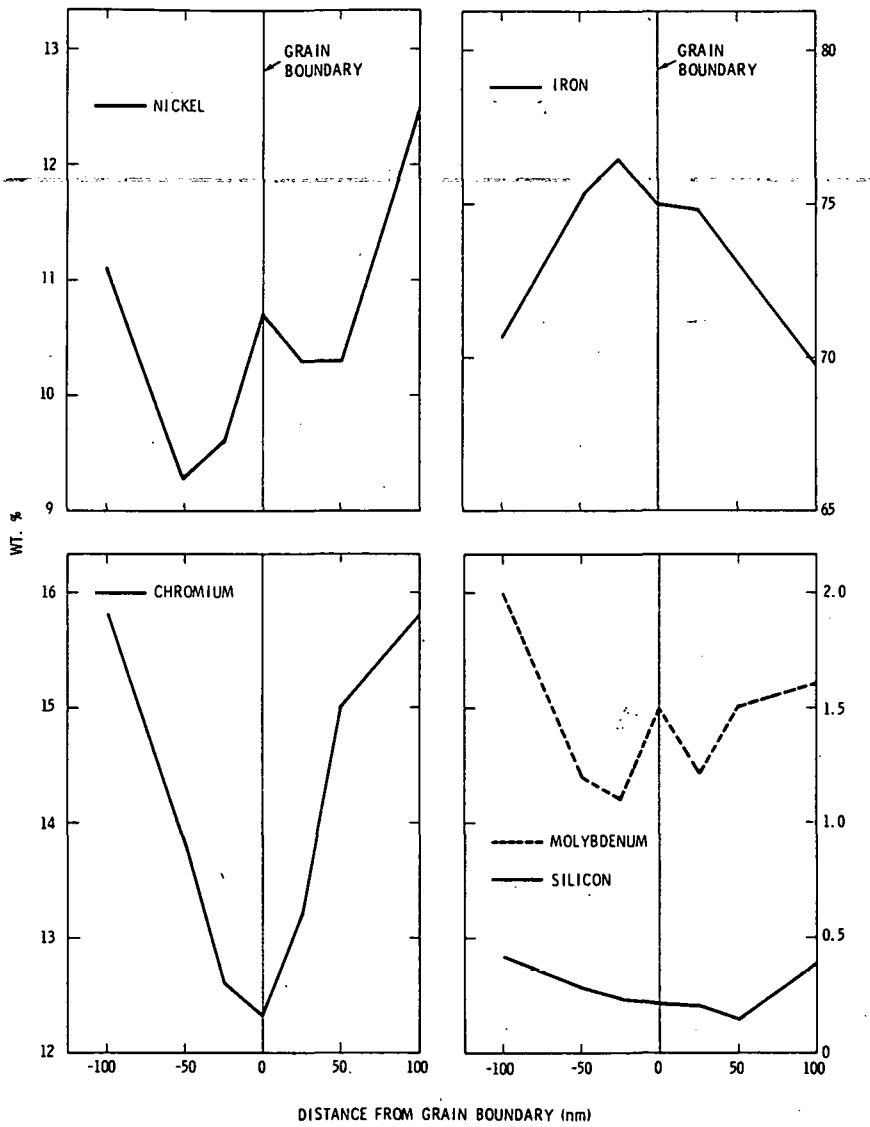

Fig. 10 - Line-of-sight measurements (4) of elemental profiles in the vicinity of grain boundary of 0.5% Si alloy at 520°C and 9 x 10^{22}n/cm^2 (E >0.1 MeV).

The MV-II data at higher fluences and the results of ion bombardment studies (19) indicate that the addition of a small amount of silicon initially depresses void nucleation and manifests itself as an increased incubation period. Due to the associated removal of nickel and silicon from the matrix, however, the eventual steady-state swelling rate increases with increasing initial silicon content (12). The benefit of reduced swelling gained by extending the incubation period will be overwhelmed at some high fluence as the higher swelling rate overtakes that of a lower silicon alloy with a shorter incubation period. This explains the first reversal of swelling behavior shown in Figure 7.

When the matrix nickel level falls to very low levels, the austenite is predisposed toward a transition to ferrite, a phase which is known to resist swelling. Thus the highest initial swelling rate is attained by austenite which will shortly become low-swelling ferrite. This explains the second reversal shown in Figure 7 and accounts for the maximum observed in swelling at 1.5 wt.% silicon. It should be noted that the peak density change as a

measure of swelling is distorted somewhat by the transformation itself, since the ferrite is about 2% less dense than the austenite. The transformation of 316 stainless steel to ferrite during irradiation was also observed by Porter and Wood (8).

At the nominal silicon level of 0.5 wt.%, no ferrite was observed at 620°C and 12.0 x 10^{22} n/cm^2 (E >0.1 MeV). The matrix nickel level had fallen to about 11%. In the 1.96 wt.% Si alloy the austenite matrix nickel content had fallen to about 6% and substantial ferrite formation had occurred. Similar trends were observed to a lesser extent in the 1.5 wt.% Si alloy. It therefore appears that 1.0 wt.% silicon eventually results in the removal of at least 3 to 4 wt.% nickel from the matrix. Other studies (3,6) appear to indicate that the ferrite transition level occurs when the matrix nickel concentration is below 10 wt.% since no detectable ferrite has been observed in specimens reaching this nickel level at comparable fluences and initial silicon levels.

The failure to observe ferrite in the 0.48% silicon specimen does not mean that ferrite does not exist. Porter and Wood (8) have observed ferrite to form in both annealed and cold-worked 316 stainless steel at 550°C, but the volume fraction of ferrite was small. At other temperatures no ferrite was detected. More importantly, Stanley and Hendrickson (20) showed that small ferrite particles in AISI 316 were undetectable by microscopy, although magnetic measurements clearly demonstrated their existence. In AISI 321 a much higher level of magnetism and ferrite concentration (4 to 5%) was found by these investigators; the ferrite particles were only 10 nm in diameter.

The question arises whether the $\gamma \rightarrow \alpha$ transformation occurs by a nucleation and growth process during irradiation or by a martensitic inversion upon cooling. Porter (21) has deduced that the transformation is a continuous process involving nucleation and growth on stacking faults, citing as evidence the nature of the $\gamma \rightarrow \alpha$ boundaries and the absence of twinning in the α-phase. Mazey and coworkers (22) arrive at the opposite conclusion from an ion irradiation study of a series of 12Cr-15Ni-Fe alloys. Their conclusion was based on the observation that the matrix nickel content was reduced by precipitation of Ni_3Si and other phases, which should lead to an increase in the martensitic transformation temperature. They also note that X-ray analysis shows the remaining austenite and the ferrite have essentially identical compositions, whereas they would expect substantially different nickel or nickel equivalent compositions for a diffusion and growth process. Mazey also notes that voids were found in the ferrite regions which are known to resist swelling.

Our results also show reduced and essentially identical concentrations in the two phases as well as the absence of any martensitic structure. However, it is felt that the diffusion and growth process cannot be rejected because of the presence of voids in ferrite or the identical levels of nickel in each phase. The voids were initially formed in austenite regions which later transformed to ferrite, leaving austenite shells around voids. If the silicon level is high enough, these shells can shrink away, leaving the voids encased in ferrite. The identical nickel levels of the austenite and ferrite regions could merely indicate that the remaining austenite is close to transforming also. The possible error in the alternate rationale might lie in ignoring the fact that other precipitate phases are the reservoir for the depleted nickel.

The role of surfaces as a sink for nickel is reflected not only in the retention of austenite shells around voids in high silicon alloys but also in the concentration profiles measured near void surfaces in low silicon alloys and near grain boundaries in alloys with moderate silicon content.

It is interesting to note that the driving force for nickel removal appears to reside with the nickel itself rather than its interaction with elements such as silicon. In the alloy with virtually no silicon, the voids were still capable of reducing the matrix nickel content somewhat. As shown in other papers (4,5) the segregation of nickel (and not silicon) occurs at the expense of primarily chromium and secondly iron. Nickel is the slowest and chromium the fastest diffusing component of Fe-Ni-Cr ternary alloys.(23,24) Silicon in these alloys posesses a diffusivity two to three orders of magnitude greater than that of iron, nickel or chromium.(28) The segregation of nickel but not silicon to void surfaces appears to indicate that one of the major driving forces for the microchemical evolution is the Inverse Kirkendall effect (25), wherein the slowest-diffusing species segregate by default at the bottom of vacancy gradients.

However, there is evidence from many studies that the gradients in interstitial concentration around microstructural sinks also lead to segregation. It is thought that atoms with smaller sizes tend to form longer-lasting mixed-dumbells with irradiation produced interstitials. Nickel has the smallest partial molar volume of Fe-Ni-Cr-Si alloys in the 300 series stainless steels and silicon has the next smallest volume.(26) Therefore both elements should flow down interstitial gradients. Silicon therefore flows down interstitial gradients and up vacancy gradients associated with each sink, while nickel flows toward the sink on both gradients. The two flows of silicon must be closely balanced in this alloy since silicon does not segregate to the net vacancy sink (void) but does segregate at a net interstitial sink (Frank loop).(12,16)

Several additional points should be made about the precipitate phases observed in these steels. In the high silicon alloys γ' was found at 620°C, whereas it is known to exist only at <540°C in typical heats of AISI 316 which contain about 0.5% silicon. Extension of the γ' stability regime to higher temperatures with either increasing solute or displacement rate is expected on the basis of theoretical considerations (27). The absence of enrichment of nickel and silicon in the precipitates observed in the 0.5% silicon specimens irradiated at 510°C is in contrast with the behavior observed at all other temperatures. It is consistent, however, with the observation that swelling exhibits a minimum at this temperature, which produced the "double bump" swelling behavior typical of annealed 316 stainless steel (12).

Conclusions

The irradiation of AISI 316 leads to an extensive repartition of several elements, particularly nickel and silicon, between the matrix and various precipitate phases. The segregation of nickel at free surfaces at the expense of the faster-diffusing elements is a clear indication that one of the operative mechanisms is the Inverse Kirkendall effect. Nickel is also expected to segregate to microstructural sinks due to solute drag with mixed dumbell interstitials. However, silicon segregation is dictated by the competition of its interactions with both vacancies and interstitials, and therefore varies for each type of microstructural component.

At low silicon levels, increasing the silicon content decreases void nucleation and leads to an increased incubation fluence. Increases in the silicon content above 0.5% reduce the matrix nickel content by increasing the formation of several nickel and silicon-rich phases. This causes the alloy matrix to swell eventually at higher rates than observed at lower silicon levels. Large additions of silicon cause progressively larger fractions of the austenite matrix to transform to ferrite as the matrix nickel level declines. The transformation is resisted near void surfaces which are richer in nickel.

References

1. H. R. Brager and F. A. Garner, J. Nucl. Mat., 73 (1978), p. 9.

2. H. R. Brager and F. A. Garner, Trans ANS, 28 (1978), p. 151.

3. H. R. Brager and F. A. Garner, "Dependence of Void Formation on Phase Stability in Neutron-Irradiated Type 316 Stainless Steel," Effects of Radiation on Structural Materials, ASTM STP 683, J. A. Sprague and D. Kramer (Eds), ASTM (1979), pp. 207-232.

4. H. R. Brager and F. A. Garner, "Analysis of Radiation-Induced Microchemical Evolution in 300 Series Stainless Steel," Proceedings of Symposium on Advanced Techniques for the Characterization of Irradiated Materials, February 24-28, 1980, Las Vegas, Nevada, to be published in J. Nucl. Mat.

5. H. R. Brager and F. A. Garner, "Microchemical Evolution of Neutron-Irradiated 316 Stainless Steel," Effects of Radiation on Materials, ASTM STP 725, D. Kramer, H. R. Brager and J. S. Perrin (Eds), ASTM (1981).

6. W. J. S. Yang, H. R. Brager and F. A. Garner, "Radiation-Induced Phase Development in AISI 316," this conference.

7. C. Cawthorne and C. Brown, J. Nucl. Mat., 66 (1977), p. 201.

8. D. L. Porter and E. L. Wood, J. Nucl. Mat., 83 (1979), p. 90.

9. P. J. Maziasz, Scripta Met., 13 (1979), p. 621.

10. P. J. Maziasz, J. Nucl. Mat., 85 and 86 (1979), p. 713.

11. P. J. Maziasz, "Precipitation Response of Austenitic Stainless Steels to Simulated Fusion Irradiation," in The Metal Science of Stainless Steels, E. W. Collins and H. W. King (Eds), Proceedings, 107th AIME Annual Meeting, Denver, Colorado, March 2, 1978.

12. F. A. Garner, "The Microchemical Evolution of Irradiated Stainless Steels," this conference.

13. F. A. Garner, E. R. Gilbert, D. S. Gelles and J. P. Foster, "The Effect of Temperature Changes on Swelling and Creep of AISI 316 Stainless Steel," ibid. Ref. 5.

14. F. A. Garner, E. R. Gilbert and D. L. Porter, "Stress-Enhanced Swelling of Metals During Irradiation," ibid. Ref. 5.

15. G. D. Johnson, F. A. Garner, H. R. Brager and R. L. Fish, "A Microstructural Interpretation of the Fluence and Temperature Dependence of the Mechanical Properties of Irradiated AISI 316," ibid. Ref. 5.

16. F. A. Garner and W. G. Wolfer, "The Effect of Solute Additions on Void Nucleation," accepted for publication in J. Nucl. Mat., also University of Wisconsin Report UWFDM-391, September 1980.

17. J. F. Bates, "Irradiation-Induced Swelling Variations Resulting from Compositional Modifications of Type 316 Stainless Steel," Properties of Reactor Structural Alloys After Neutron or Particle Irradiation, ASTM STP 570, American Society for Testing and Materials (1975), pp. 369-387.

18. J. F. Bates, R. W. Powell and E. R. Gilbert, "Reduction of Irradiation-Induced Creep and Swelling by Compositional Modifications," ibid. Ref. 5.

19. J. F. Bates and W. G. Johnston, "Effects of Alloy Composition on Void Swelling," Proceedings, Radiation Effects on Breeder Reactor Structural Materials, M. L. Bleiberg and J. W. Bennett (Eds) TMS-AIME (1977), p. 625.

20. J. T. Stanley and L. E. Henrickson, J. Nucl. Mat., 80 (1979), p. 69.

21. D. L. Porter, J. Nucl. Mat., 79 (1979), p. 406.

22. D. J. Mazey, D. R. Harries and J. A. Hudson, "The Effect of Silicon and Titanium on Void Swelling and Phase Stability in 12Cr-15Ni-Fe Alloys Irradiated with 46 MeV Nickel Ions," to be published in Proceedings of International Conference on Irradiation Behavior of Metallic Materials for Fast Reactor Core Components, Ajaccio, Corsica, June 4-8, 1979.

23. W. Assassa and P. Guiraldenq, Metal Sciences, (March 1973), p. 123.

24. S. J. Rothman, L. J. Nowicki and G. E. Murch, J. Phys. F: Metal Physics, 10, (1980) 383-398, also "Tracer Diffusion of Cr, Ni and Fe in Austenitic Fe-Cr-Ni Alloys," presented at Fall AIME Meeting, St. Louis, MI, (October 15-19, 1978).

25. P. R. Okamoto and L. E. Rehn, J. Nucl. Mat., 83 (1979), p. 2.

26. J. L. Straalsund and J. F. Bates, Met. Trans., 5 (1974), p. 1493.

27. G. Martin, J. L. Bocquet, A. Barbu and Y. Adda, "Fundamental Aspects of the Evolution of, and Phase Changes in, Metals and Alloys Under Irradiation," ibid. Ref. 20, p. 899.

28. R. A. Swalin, A. Martin and R. Olsen, Trans. AIME, (1957) p. 936.